Volume 55
Number 6
10 February 2026
Pages 2349-2730

Dalton Transactions

An international journal of inorganic chemistry

rsc.li/dalton

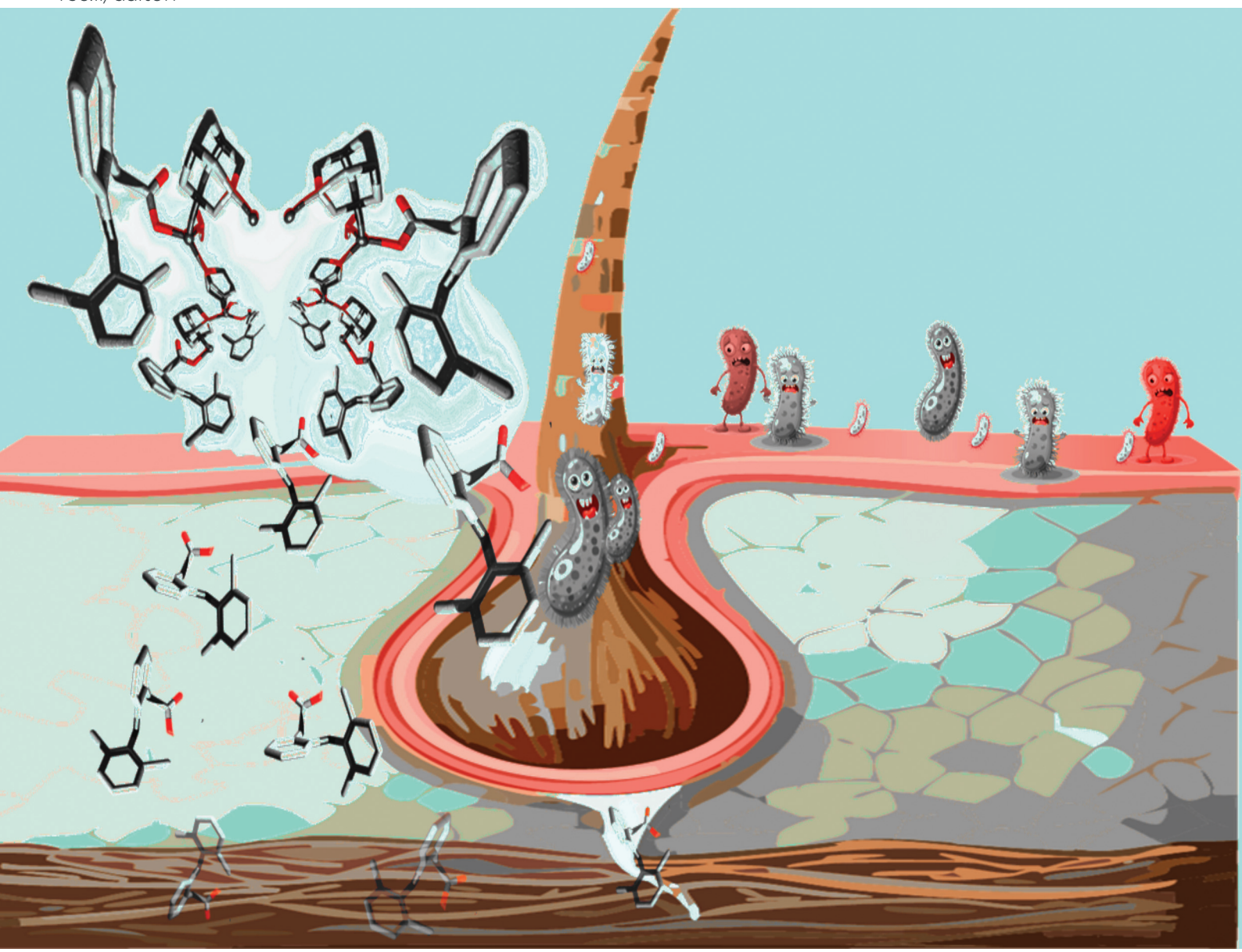

ISSN 1477-9226

ROYAL SOCIETY OF CHEMISTRY

PAPER

Sabina W. Jaros, Bożena Michniak-Kohn *et al.*
Silver(I) coordination polymer meets chia seed mucilage based film – antimicrobial performance and evaluation of permeability trends through human skin *in vitro*

Dalton Transactions

ROYAL SOCIETY OF CHEMISTRY

PAPER

View Article Online
View Journal | View Issue

Cite this: *Dalton Trans.*, 2026, **55**, 2443

Silver(I) coordination polymer meets chia seed mucilage based film – antimicrobial performance and evaluation of permeability trends through human skin *in vitro*

Sabina W. Jaros, *[a] Justyna Markieton, [a] Magdalena Florek,[b] Jarosław Król,[b] Seeprarani Rath, [d] Sesha Rajeswari Talluri,[c,d] Nubul Albayati[c,d] and Bożena Michniak-Kohn*[c,d]

Antimicrobial resistance is one of the critical threats, resulting in nearly 3500 deaths every day, jeopardizing the health system globally. This alarming issue demands urgent attention and action in the form of designing and generating new, effective disinfecting and therapeutic materials. Herein, we present a new chia seed-based film (CSM) and CSM-doped with therapeutic 1D coordination polymer $[Ag(\mu\text{-PTA})(Df)(H_2O)]_n \cdot 3nH_2O$ (**1**) (**composite 1@CSM**). Both compound **1** and its **composite 1@CSM** revealed a broad spectrum of antimicrobial action, with complete halting of the growth of clinically significant pathogenic microorganisms *E. coli*, *S. aureus*, and *C. albicans*. Simultaneously, *in vitro* drug permeation analysis of **1** using human cadaver skin as a membrane revealed the potential for topical delivery of antimicrobial compound **1** for localized action in the upper layers of the epidermis, specifically the stratum corneum, and the transdermal delivery of diclofenac sodium (a nonsteroidal anti-inflammatory drug, NSAID). This development not only opens the door to the exploration of Ag(I)-based coordination polymers as promising transdermal drug delivery systems, but it also significantly enhances the narrow field of therapeutic coordination polymers that exhibit synergistic effects of antimicrobial, anti-inflammatory, and demulcent action.

Received 16th October 2025,
Accepted 22nd December 2025

DOI: 10.1039/d5dt02494c

rsc.li/dalton

Introduction

Effective treatment and prevention of infections, along with comprehensive pain management and mitigation, are essential pillars that significantly impact the well-being of humans globally. Recently, much effort has been directed towards designing advanced therapeutic materials for wound treatment and pain management based on metal–organic frameworks (MOFs) and coordination polymers (CPs). CPs, especially those exhibiting bioactivities, are the subject of extensive research and serve as a platform for developing advanced therapeutic materials.[1–6] New delivery systems for diclofenac that utilize CPs are emerging as promising drug delivery therapeutic agents. These systems may offer potential synergistic effects that enhance anti-inflammatory, antimicrobial, and wound-healing properties. Their application in dermal and transdermal drug delivery presents an encouraging avenue for medication administration.[7–9] This approach offers a range of advantages, including the ability for programmed and controlled drug delivery over extended time periods, the avoidance of first-pass metabolism, and enhanced comfort for patients, particularly those managing chronic or infected wounds.[7–10] However, designing a transdermal drug delivery system remains challenging due to the skin's protective function and its diffusion-barrier role. Moreover, in light of the growing issue of antimicrobial resistance to conventional antibiotics,[11] the utilization of new silver-based antibacterial materials and their application in transdermal drug delivery systems presents a viable alternative for established treatment options, especially for infected and oozing wounds.

The acidic form of diclofenac is characterized as a lipophilic nonsteroidal anti-inflammatory drug (NSAID), with documented low bioavailability when administered orally, and unwanted side chemical transformation under heating, acidic

[a]*Faculty of Chemistry, University of Wroclaw, F. Joliot–Curie 14, 50-383 Wrocław, Poland. E-mail: sabina.jaros@uwr.edu.pl*
[b]*Department of Pathology, Division of Microbiology, Wrocław University of Environmental and Life Sciences, Norwida 31, Wrocław, Poland*
[c]*Ernest Mario School of Pharmacy, Rutgers-The State University of New Jersey, 160 Frelinghuysen Road, Piscataway, NJ 08854, USA. E-mail: michniak@pharmacy.rutgers.edu*
[d]*Center for Dermal Research, Rutgers-The State University of New Jersey, 145 Bevier Road, Piscataway, NJ 08854, USA*

media, ultrasound, or light irradiation is related to the serious side effects associated with the formation of stomach ulcers or gastric irritation.[12,13] Therefore, transdermal drug delivery systems present significant advantages and are increasingly regarded as valuable and desirable in the development of new advanced therapeutic materials. One of the key benefits of transdermal diclofenac delivery is the avoidance of the gastrointestinal route for administration. This minimizes the potential for unwanted effects that can arise in the digestive system, thereby enhancing patient safety and comfort.

In 2024, Murphy *et al.* elucidated a new and intriguing subclass of CPs identified as therapeutic coordination polymers (TCPs).[7] This group encompasses non-porous coordination polymers that reveal drug release through degradation of the metal–ligand bond. Recently, we presented one-dimensional silver(I) coordination polymers composed of 1,3,5-triaza-7-phospaadamantane (water-soluble linker, referred to as PTA) in combination with the diclofenac (Df) anion (widely applied in demulcent, antipyretic, and anti-inflammatory therapy).[14] This drug-based coordination polymer (CP) with the general formula $[Ag(\mu\text{-PTA})(Df)(H_2O)]_n{\cdot}3nH_2O$ (**1**) demonstrated significant selectivity and cytotoxicity against human pancreatic duct carcinoma (PANC-1) cell lines, as well as degradation-based ligand release of diclofenac,[14] thereby expanding the group of therapeutic 1D coordination polymers.[8]

The lipophilicity parameter log *P* is crucial in pharmacology and describes the tendency of biomolecules to pass through physiological membranes and their affinity to lipophilic environments.[14] The experimental studies indicated that compound **1** has a log *P* value of −0.61, indicating its hydrophilic properties. In contrast, the log *P* values for HDf and NaDf are positive, measuring 4.5 and 1.4, respectively.[13] This comparison of log *P* highlights the hydrophilic profiles of **1** and characteristics suitable for transdermal delivery of the diclofenac molecule. Therefore, in this study, we wanted to explore the permeability behavior of compound **1** through human skin. Another objective was to assess the potential antimicrobial properties of the compound. Furthermore, we employed compound **1** to develop a novel antimicrobial biomaterial (Fig. 1), designated as **composite 1@CSM**, which is derived from chia seed mucilage (CSM). The CSM films are increasingly attracting interest due to their impressive swelling capabilities, which hold great potential for the development of nanocapsules, advanced wound dressings, hygienic pads/mats, and surgical gauze.[15–17] Chia seeds and CSM are easy-to-process and readily available materials, recognized for their high nutritional value.[18,19] In this work, we present a new materials that, for the first time, integrate Ag(I)-based coordination polymers and CSM hydrogel film (Fig. 2). This innovative approach paves the way for novel applications of nonporous antimicrobial Ag-CPs in dermal and transdermal drug delivery systems, as well as the development of advanced antimicrobial materials for health prevention applications.

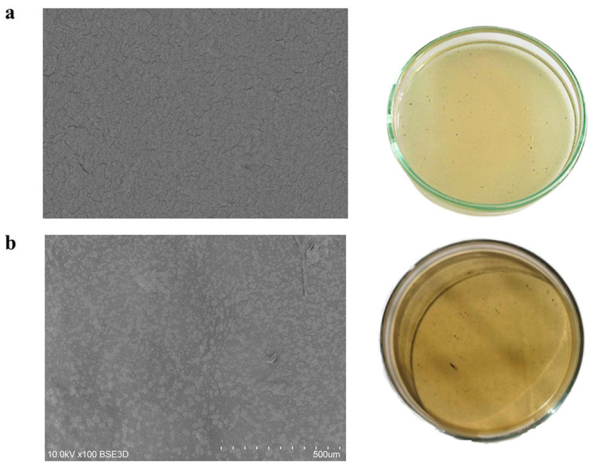

Fig. 2 The image of as-synthesized CSM (a), **composite 1@CSM** (b) films and their SEM micrographs.

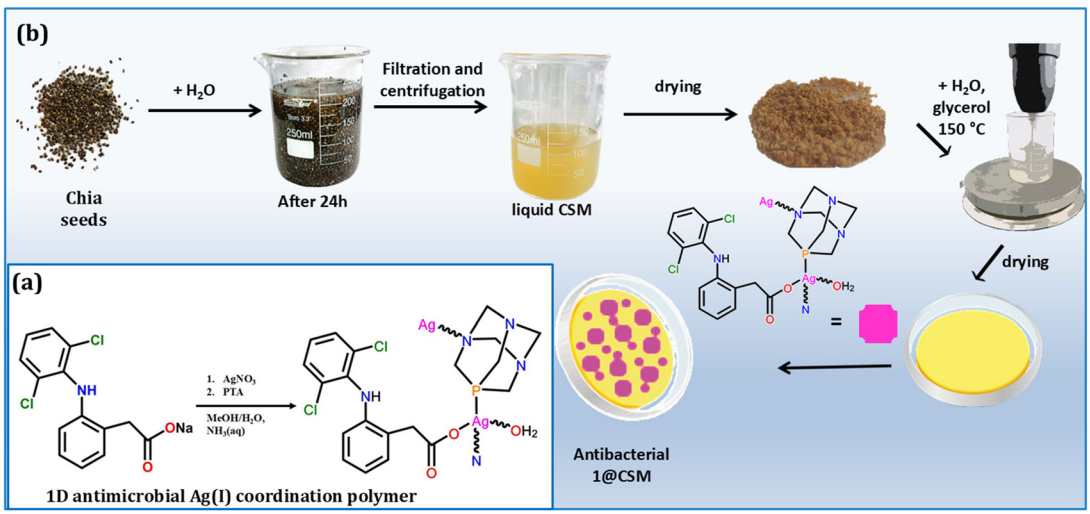

Fig. 1 General synthetic procedure for the synthesis of (a) 1D coordination polymer (compound **1**) and (b) **composite 1@CSM**.

Results and discussion

The 1D $[Ag(\mu\text{-PTA})(df)(H_2O)]_n \cdot 3nH_2O$ (**1**) coordination polymer (Fig. 1a) was prepared by the method previously published by Jaros *et al.*[14] The compound was fully characterized using spectroscopic methods (FT-IR, ^1H, $^{31}P[^1H]$ NMR) and mass spectrometry (see SI). The PXRD confirmed its crystallographic fingerprint and purity (SI, Fig. S5). The obtained experimental results are in good agreement with previously reported data for compound **1**.[14] The promising hydrophilic properties, light stability, and water solubility of compound **1** prompted us to investigate its antimicrobial potential and its permeability properties in regard to the human skin.

Moreover, we used compound **1** to generate **composite 1@CSM** material that can serve as adsorbing antimicrobial patches or mats. In the first step, we extracted CSM from the seeds. Our modified extraction procedure, which applies ultrasound irradiation, allows us to obtain dry CSM with a 4.5% yield. The most challenging part is the separation of liquid CSM from the solid residue of chia seeds (nylon gauze was used for filtration). A dry CSM was then used as starting material for preparing CSM patches (Fig. 1b). The 0.750 mg of CSM were combined with 20 ml of distilled water, homogenized, and left for 30 minutes for gelling. Subsequently, glycerol was incorporated into the mixture, followed by thorough homogenization. The thick, yellow mixture was then heated to 150 °C for 30 minutes and transferred to a sterilized hot (160 °C) Petri dish. The CSM material was left for air drying at room temperature for 48 hours (Fig. 1).

Next, generated CSM films were utilized to prepare a hybrid antimicrobial **composite 1@CSM** films. The suspension of **1** in 2 ml of water was added to the cooled (50 °C) CSM and then homogenized for five minutes. In the final step, the obtained hot mixtures were poured into sterilized Petri dishes and dried in a vacuum dryer or air-dried for 2 to 5 days. Both CSM and **1@CSM** were characterized using FT-IR (SI, Fig. S3 and S4) and PXRD (SI, Fig. S13) analysis. The diffractograms of **CSM** and **composite 1@CSM** (SI, Fig. S13) closely match, showing the same broad peak, which indicates that both are in an amorphous state.

Film appearance, thickness, transparency, and porosity

The CSM and **composite 1@CSM** films exhibit a yellowish and transparent appearance after drying, as shown on the right side of Fig. 2. However, the colour of **composite 1@CSM** is more yellow. Both materials are flexible and do not crack during the drying process. The incorporation of glycerol into the film as a plasticizer in a concentration of 5% eliminates brittleness and provides films with an appropriate texture.

The addition of **1** does not affect the recorded overall thickness and porosity of both materials, which are in the range of 22 to 23 ± 0.004 mm and 40%, respectively (Table 1). However, it affects the final colour and degree of swelling (DG) of the obtained materials. The CSM is pale yellow, **composite 1@CSM** is dark yellow (yellowish orange). The **CSM** and **composite 1@CSM** materials have high porosity with similar values of 40.27% ± 0.45 and 40.42% ± 0.52. The obtained data are comparable to those observed by Zawar *et al.* for their CSM material, which exhibits porosity at the level from 36 to 47%.[20]

Table 1 The characteristics of CSM and **composite 1@CSM** materials

Sample	Porosity (%)	Thickness (mm)	DS (%)	WRC (%)
CSM	40.27 ± 0.45	0.22 ± 0.004	138.22 ± 0.39	39.49 ± 0.27
1@CSM	40.42 ± 0.52	0.23 ± 0.004	81.94 ± 0.43	38.54 ± 0.27

n = 3, ±SD, DSC – degree of swelling, WRC – water retention capacity.

The SEM micrographs demonstrate that CSM and **1@CSM** materials are rather smooth, but small particles (from chia casings) are visible. It should be noted that small cracks cover the surface of the CSM material and **composite 1@CSM** (SI, Fig. S7 and S8). The EDS-elemental mapping was conducted to assess the composition of the **1@CSM** materials. The results indicated the presence of silver species (SI, Fig. S9). The observations indicate that Ag, P, and Cl elements are well distributed on the surface of the **1@CSM** material. However, in some areas, larger crystalline particles of **1** can be observed locally. The overlayering of these elements suggests preservation of the coordination environment around the silver ion and the formation of nearly uniform **1@CSM** material.

Degrees of swelling (DS) and water retention capacity (WRC)

Table 1 presents an overview of the thickness of both films, along with an assessment of their swelling behaviour following 24 h of immersion in H_2O. The CSM film demonstrated a notable swelling capacity of 138.22% ± 0.39, which is probably connected to the high porosity of the material. This is related to the CSM film's hydrophilic nature. The incorporation of compound **1** and the formation of **composite 1@CSM** cause a 57% reduction in the swelling level of the obtained material. Notably, CSM and **composite 1@CSM** films exhibited similar water retention capacities of 39.49 ± 0.27% and 38.54 ± 0.27%, respectively.

FTIR analysis

The addition of compound **1** does not significantly change the structure of CSM biofilm. This is confirmed by FTIR analysis (SI, Fig. S1–S4). The FT-IR spectra of CSM and **composite 1@CSM** films were reported in the range of 4000 to 400 cm^{-1} and are presented in Fig. S3 and S4 (SI). The band in the range from 3409 to 3401 cm^{-1} corresponds to the stretching of the OH-group. The stretching vibrations observed in the range of 1643 to 1633 cm^{-1} for **composite 1@CSM** and CSM, respectively, represent a significant characteristic region of protein

structure, which can be attributed to the amide I band. This band is related to the C=O vibration, and its frequencies depend on the nature of the hydrogen bond between the C=O and NH components of the peptide linkages.[20–23] The bands characteristic of the uronic acid and its C–H vibration are observed at 1416 and 1417 cm^{-1} for CSM and **composite 1@CSM**. The vibration at 1045 cm^{-1} is characteristic of hemicellulosic moieties and indicates its COC glycosidic linkage. The addition of CPs **1** does not significantly change the structure of CSM biofilm. However, the broader band at 3401 cm^{-1} observed on the spectra of **composite 1@CSM** suggests the occurrence of intermolecular interaction assigned to the hydrogen bond. It was observed that the more complex the hydrogen system was, the broader the OH vibration became.[20–23]

Antifungal and antibacterial activity assessment

Antibacterial tests were performed for compound **1** using the serial dilutions method. The estimated Minimal Inhibitory Concentration (MIC) was expressed in μg mL^{-1} (Table 2).[24] The lowest values of MIC were detected for the two Gram-negative bacteria, *Escherichia coli* (6 μg mL^{-1}) and *Pseudomonas aeruginosa* (7 μg mL^{-1}). *Staphylococcus aureus* (the Gram-positive bacterium) and *Candida albicans* (a fungus of the yeast group) was less susceptible to the compound tested, with MIC values of 10 and 40 μg mL^{-1}, respectively. Overall, compound **1** exhibits superior antimicrobial activity compared to the standard reference antimicrobial agent, silver nitrate. When theMIC is expressed as a normalized MIC [nmol mL^{-1}], compound **1** demonstrates activity four to five times greater for the Gram-negative bacteria and over three times higher for the yeast than the $AgNO_3$. The most significant difference observed is a seven times higher activity of compound **1** against the Gram-positive bacterium *S. aureus* compared to that of the reference salt. The mass spectrometry tests of compound **1** show that, in solution, there is formation of $[Ag(PTA)_2]^+$ and $[Ag_2(PTA)_2(Df)]^+$ lower mass species (SI, Fig. S12), indicating that the polymeric structure is not maintained in solution. The presence of lower-mass species aligns well with previously reported results for Ag(I)-PTA derivatives.[14,23,25–28] The collective results from various ESI-MS tests indicate that the $[Ag(PTA)_2]^+$ species in solution is the most stable ion. Additionally, this ion in the presence of Cl^- ions may form $[Ag_2(PTA)_2Cl]^+$ species.[28] The coordination of the chloride ligand may significantly increase lipophilicity, enhance stability, and influence permeation through the bacterial lipid layer of Ag(I) species, ultimately leading most probably to the effective bacterial eradication and enhanced antimicrobial action. The release of diclofenac anion is also observed.[14] Given the notable and broad spectrum of antimicrobial efficacy, compound **1** was employed to develop a new antimicrobial film, **composite 1@CSM**.

Table 2 MICs and normalized MIC of compound **1** against pathogenic bacteria and yeasts tested in the present study

MIC [μg mL^{-1}]			Normalized MIC[a] [nmol mL^{-1}]	
Microorganism	**1**	$AgNO_3$	**1**	$AgNO_3$
Gram-negative bacteria				
Escherichia coli	6	9	10	53
Pseudomonas aeruginosa	7	9	12	53
Gram-positive bacteria				
Staphylococcus aureus	10	20	17	118
Yeasts				
Candida albicans	40	40	69	236

[a] MIC normalized for a molar content of silver.

Evaluation of *in vitro* permeation using human skin *in vitro*

As a consequence of the detected antimicrobial activity and negative log *P* value[14] of compound **1**, *in vitro* permeation studies were performed. The permeation study of **1** in different solvent systems revealed that compound **1** dissolved in DMSO + Transcutol exhibited no measurable permeation after 72 hours, as shown in Fig. 3. Similarly, the pure drug dissolved in DMSO + Transcutol demonstrated minimal permeation, with the first detectable peak appearing only at 24 hours (Fig. 3). In contrast, the pure drug and compound **1** dissolved in DMSO + PBS (pH 7.4) exhibited enhanced permeation, with the pure drug showing slightly superior permeation compared to compound **1** (Fig. 3 and 4).

Furthermore, when suspended in PBS (pH 7.4), the pure drug and compound **1** showed the highest permeation rates among all the solvent systems tested (Fig. 4). This trend was consistent, with the pure drug in PBS (pH 7.4) exhibiting better permeation than the drug-loaded **1** in the same medium (Fig. 4).

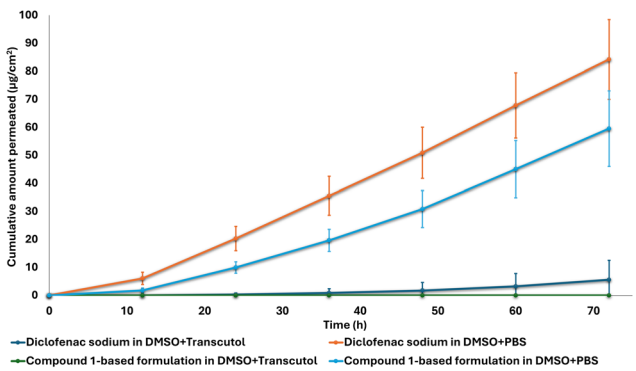

Fig. 3 Permeation profiles for the IVPT runs using diclofenac sodium and compound **1**, individually suspended/dissolved in PBS pH 7.4 and DMSO + PBS pH 7.4.

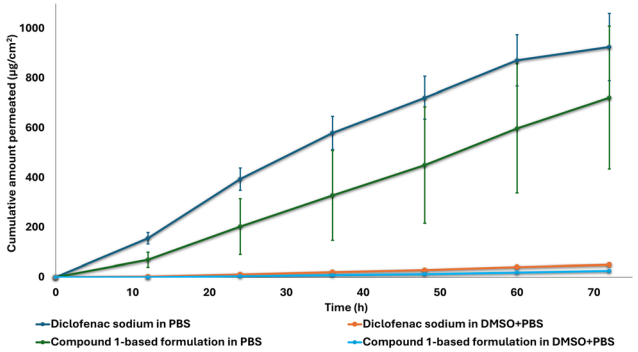

Fig. 4 Permeation profiles for the IVPT runs using diclofenac sodium and compound **1**, individually suspended/dissolved in DMSO + transcutol and DMSO + PBS pH 7.4.

All compound **1**-based formulations showed higher diclofenac sodium levels in the epidermis compared to their pure drug counterparts (Fig. 5), indicating enhanced drug deposition.

The amount of drug in the dermal layers was almost similar for the drug solution and the compound **1**-based formulation containing PBS alone. However, the compound **1**-based formulations prepared in DMSO + PBS and DMSO + Transcutol showed higher drug amounts in the dermis than their pure drug counterparts. Overall, the drug suspension in PBS showed the highest permeation, followed by the compound **1**-based formulation in PBS.

When a formulation is intended for transdermal delivery, an optimal vehicle should facilitate the drug's passage through the stratum corneum to achieve adequate flux. From a transdermal delivery standpoint, an optimal solvent system should facilitate adequate drug flux across the stratum corneum to achieve therapeutic concentrations while maintaining formulation stability, skin integrity, and patient safety.[29–31] Excessive permeability may lead to uncontrolled systemic absorption, which is undesirable for formulations intended for local action.[30,31]

In this study, formulations in phosphate-buffered saline (PBS) promoted higher permeation compared to those containing DMSO and Transcutol, suggesting that the moderate hydrophilicity of PBS supports favorable partitioning of the moderately lipophilic diclofenac sodium into and across the skin. Conversely, the reduced permeation from DMSO + Transcutol systems likely reflects excessive solubilization of the drug within the vehicle, which diminishes its thermodynamic activity and thus its driving force for diffusion.[29,32–34] Therefore, the permeability profile observed with PBS-based formulations represents a desirable balance for transdermal applications, wherein they provide sufficient flux through the skin while maintaining local drug deposition within the epidermis to support topical antimicrobial action.[31–34]

Evaluation of the surface antimicrobial properties of silver-doped biopolymers

The surface antimicrobial activity tests of CSM and **composite 1@CSM** were conducted to further investigate their biological activity.[28] The results showed that the plain polymer CSM, which was not supplemented with compound **1** (Fig. 2), showed no antimicrobial activity. Rather, all the microorganisms tested were even able to multiply on CSM discs, attaining (after 24 h incubation) numbers approximately one hundred times those detected at T_0 (Table 3).

Supplementation of the tested CSM film with compound **1** and the generation of **composite 1@CSM** enabled the material to acquire antimicrobial properties. Despite the apparently opposite action of CSM and the compound **1** in the new material **composite 1@CSM**, it exhibited pronounced inhibitory properties, resulting in the complete halting of the growth

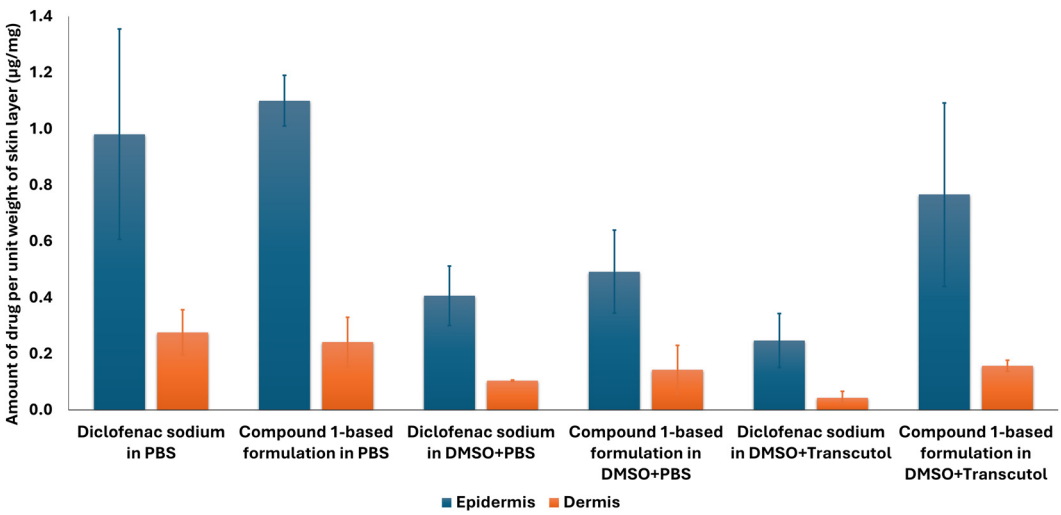

Fig. 5 Amount of diclofenac sodium detected in the epidermal and dermal layers at the end of the 72 h IVPT run.

Table 3 Number of bacteria recovered from the surface of the tested patches before (T_0) and after 24 h-long (T_{24}) incubation

	CSM		composite **1**@CSM	
Microorganism	T_0	T_{24}	T_0	T_{24}
Escherichia coli	3.2×10^3	$>3.0 \times 10^5$	2.4×10^3	**0**
Pseudomonas aeruginosa	1.3×10^4	$>3.0 \times 10^6$	9.6×10^3	7.9×10^2
Staphylococcus aureus	7.6×10^3	2.0×10^6	7.0×10^3	**0**
Candida albicans	7.8×10^1	3.8×10^3	6.9×10^1	**0**

of *E. coli*, *S. aureus*, and *C. albicans* (Table 3) over a 24 h test period. Only *P. aeruginosa* survived on **composite 1@CSM** discs, although the number of bacteria was reduced by 90%. The results align with existing literature regarding the innate resistance of *P. aeruginosa* bacteria to numerous environmental factors and chemotherapeutics.[35,36]

The mechanism underlying the antimicrobial efficiency is likely related to the gradual release of silver ions from the Ag-PTA-based coordination polymer and their penetration through the lipid bilayer of the bacterial membrane. The release of silver ions from the **composite 1@CSM** film occurs gradually in PBS, with the concentration of Ag + ions remaining constant over time, as demonstrated by the silver release tests (SI, Fig. S6). Within the 24 h period, the **composite 1@CSM** released 0.038 mg of silver ions. The release of Ag^+ maintains a consistent concentration over 8 to 24 hours, showing a slight increase after 24 hours. This concentration effectively reduces the growth of *P. aeruginosa* and completely inhibits the growth of *E. coli*, *S. aureus*, and *C. albicans* strains. Both compound **1** and **composite 1@CSM** film demonstrate notable antimicrobial activity. This finding highlights an opportunity to explore the use of **composite 1@CSM** as an efficient therapeutic patch that may offer synergistic benefits, including antimicrobial, anti-inflammatory, and pain-relieving actions in the case of wound dressing patches or antimicrobial adsorbing mats in histopathological and histochemical laboratories, mortuaries, and funeral homes. These potential applications may contribute positively to the development of antimicrobial therapeutic accessories for broad health prevention applications.

Conclusion

In summary, the present work demonstrates the antimicrobial activity and skin permeability properties of a therapeutic 1D silver(I) coordination polymer, providing an innovative approach for designing new multifunctional drug delivery systems. The experimental data revealed significant antimicrobial efficiency of compound **1** against clinically relevant pathogenic microorganisms (*E. coli*, *P. aeruginosa*, *S. aureus*, and *C. albicans*). Interestingly, *in vitro* drug permeation analysis of compound **1** using human cadaver skin as a membrane demonstrated its potential for topical delivery of antimicrobial compound **1** for local action in the upper layers of epidermis, *i.e.*, stratum corneum, as well as transdermal delivery of diclofenac sodium, a nonsteroidal anti-inflammatory drug. Furthermore, compound **1** was used to supplement chia seed mucilage (CSM) films, thereby designing a new composite material, **1@CSM**, with antimicrobial properties. To the best of our knowledge, this is the first example of CSM-based materials supplemented with Ag(I) coordination polymer. This development not only presents an opportunity to explore Ag(I)-based coordination polymers as potential transdermal drug delivery systems but also contributes to the broader group of recently reported therapeutic coordination polymers that exhibit synergistic effects, including antimicrobial, anti-inflammatory, and demulcent actions.[7] Moreover, the described **composite 1@CSM** material may contribute to designing new adsorbing antimicrobial patches and mats for health technologies.

Experimental section

Materials, reagents, and general methods

List of chemicals and materials used: chia seeds from the local market, $AgNO_3$ (Sigma-Aldrich), 1,3,5-triaza-7-phospaadamantane (Sigma-Aldrich), glycerine (Sigma-Aldrich), phosphate-buffered saline tablets (PBS, pH = 7.4, Sigma-Aldrich). Film thickness was measured using a digital calliper. Measurements were repeated three times (n = 3) in different parts of the discs. The FTIR spectra (4000–400 cm^{-1}) were measured on a Bruker Vertex 70 FTIR instrument. The used abbreviations: vs, very strong; s, strong; m, medium; w, weak; br, broad. The PXRD measurements were conducted using a Malvern Panalytical Aeris X-ray diffractometer with Cu Kα (1.5418 Å) radiation. Data were collected at room temperature within the 2θ range of 5–90°.

CSM hydrogel extraction

The chia seeds were rinsed twice with distilled water, then immersed in hot water at 60 °C at a 1 : 20 ratio, mixed, and placed in an ultrasonic bath for 2 hours. After 24 h, the hydrogel was separated from the seeds by squeezing through a nylon cloth and centrifuged for 30 min at room temperature. Then, the CSM hydrogel was dried in a dryer for 2 to 4 h (50 °C) or under nitrogen for 1 day. Yield 4.5 g (n = 3 *ca.* ~4.5%) IR (KBr, cm^{-1}): 3456 (vs br) $\nu(H_2O + OH)$, 2926 (m), 2856 (w), 1630 (s), 1527 (w), 1417 (m), 1250 (w), 1044 (vs), 883 (w), 648 (w), 538 (w), 482 (w).

Synthesis of compound 1

Compound **1** was synthesized using the procedure described by Jaros *et al.*[14] The pinkish-white microcrystalline compound **1** was obtained in a 40% yield (relative to $AgNO_3$). IR (KBr, cm^{-1}): 3231 (w), 1586 (s), 1451 (vs), 1362 (m), 1294 (m), 1241 (m), 1104 (w), 1017 (s), 971 (s), 951 (s), 775 (w), 742 (s), 597

(m), 579 (m). PXRD Analysis (SI, Fig. S7). ^{1}H NMR (500 MHz, DMSO-d_6) δ 3.49 (s, CH_2COO, 2H, Df), 4.23 (d, $2J_{P-H}$ = 2.69 Hz, 6H PCH_2N, PTA) 4.39 and 4.55 (d, J = 12.59 Hz, 6H NCH_AH_BN, PTA) 6.27 (d, J = 7.82 Hz, 1, C_6H_4, Df) 6.78 (dt, J = 7.44 and 1.1 Hz, 1H, C_6H_4, Df) 6.97 (dt, J = 7.63 and 1.53 Hz, 1H, C_6H_4, Df) 7.07 (d, J = 7.6 Hz, 1H, C_6H_4, Df), 7.13 (t, J = 8.0 Hz 1H, C_6H_3, Df) 7.48 (d, J = 8.20 Hz, 2H, C_6H_3, Df), 9.21 (s, 1H, NH, Df). ^{31}P[^{1}H] NMR (DMSO-d_6, 202.5 MHz): −83.46 (s, PTA). ESI-MS (±) (CH_3OH/H_2O), MS(+) m/z: 421.05 (100%) $[Ag(PTA)_2]^+$, 823.95 (20%) $[Ag_2(PTA)_2(Df)]^+$.

Preparation of the CSM

The dry CSM was soaked in distilled water (2.7% of total weight), homogenized, and left for 20 minutes. Then the mixture of CSM was mixed with hot glycerine (5% w/w as a plasticizer for 30 min (150 °C)). The transparent yellowish gel was poured into a sterilized Petri dish and allowed to air dry at room temperature (2–4 days) or in a dryer for 4–5 h at 40 °C. IR (KBr, cm^{-1}): 3409 (vs, br) ν(H_2O + OH), 2935 (w), 1633 (s), 1416 (m), 1114 (s), 1045 (s), 994 (w), 925 (m), 859 (m), 567 (w), 416 (w).

Preparation of composite 1@CSM

The dry CSM (1.5 g) was soaked in distilled water (40 mL), homogenized, and left for 20 minutes. Then the mixture of CSM was mixed with hot glycerine (5% w/w as a plasticizer for 30 min (500 revolutions, 150 °C)). The temperature was reduced to 50 °C, a suspension of 5 mg (**1**) in 2 mL of water was added, and stirred for 5 min. The transparent yellow gel was poured into a sterilized Petri dish (9 cm) and allowed to air dry at room temperature (2–4 days) or in a dryer for 4–5 h at 40 °C. IR (KBr, cm^{-1}): 3401 (m, br) ν(H_2O + OH), 2940 (w), 1643 (m), 1417 (m), 1235 (w), 1112 (vs), 1045 (vs), 993 (w), 855 (m), 675 (w), 563 (w).

In vitro permeation testing of compound-1-based formulations

In vitro permeation testing (IVPT) method

In vitro permeation testing (IVPT) studies were performed using a VDC system (Logan Instruments, NJ) consisting of VDCs (volume: 5 mL, orifice: 0.9 mm) with open donor compartments, mounted on a heating block and a magnetic stirrer. Dermatomed human cadaver skin of 500 ± 100 μm thickness, kept in a freezer (−80 °C) until it is needed for the permeation study, was used. All samples are used within 6 months of being in the freezer. The donated human skin samples were purchased from a US-approved Skin Bank Science Care (Phoenix, AZ, USA). Institutional Review Board at Rutgers, the State University of New Jersey, Piscataway, NJ, USA approved the use of these skin samples – Protocol no. Pro2024000194. The skin was thawed at room temperature and cut into pieces of about 2 cm^2. Each skin piece was sandwiched between the donor and receptor compartments, having a diffusion area of 0.64 cm^2, in such a way that the stratum corneum of the skin was exposed to the donor compartment and the lower part of the skin was in contact with the receptor compartment. The receptor chamber was filled with 5 mL of Phosphate-buffered saline (PBS), pH 7.4 (10 mM), and stirred continuously at 600 rpm using a magnetic stirrer. The skin temperature was maintained at 32 °C ± 0.5 °C. The diffusion cells were allowed to equilibrate with skin for 15 min, followed by application of a pseudo-infinite dose (500 μL). To verify the integrity of the skin sample, the Trans Epidermal Water Loss (TEWL) values were measured using a Delfin vapometer, and any skin samples with values exceeding 15 g m^{-2} h^{-1} were discarded. 500 μL samples were withdrawn from the sampling ports at predetermined time points 12, 24, 36, 48, 60, and 72 h, followed by an instantaneous replenishment with the same volume of fresh receptor medium kept at 32 °C. All samples were analyzed to determine drug content using a validated HPLC method described below, and the cumulative amount of drug permeated was plotted against time to obtain the permeation profile.

At the end of the IVPT study, skin samples were gently removed from the Franz diffusion cells. The skin was then trimmed around the diffusion area using a punch corresponding to the surface area of the donor compartment (0.64 cm^2), and the dermal and epidermal layers were separated manually using tweezers. The layers were air-dried, accurately weighed, and transferred into BeadBug tubes. To extract the drug, the skin samples were cut into smaller pieces using scissors. Then, 1 mL of methanol was added to each tube to facilitate drug extraction from the skin. The samples were homogenized using a BeadBug™ Microtube Homogenizer (D1030, Benchmark Scientific, Sayreville, NJ, USA). The homogenized samples were centrifuged at 1500 rpm for 10 min and filtered through a 0.45 μm polypropylene filter to remove any skin debris. The filtered samples were then analyzed using a validated HPLC method. The amount of diclofenac sodium in the skin was determined and expressed as μg mg^{-1} of skin weight.

High-performance liquid chromatography (HPLC) method

An Agilent 1100 series high-performance liquid chromatograph (HPLC) with an autosampler, coupled with a UV detector, was used to analyze drug concentrations in all the *in vitro* permeation testing (IVPT) samples. The concentration of diclofenac sodium was measured using an Agilent Zorbax Eclipse XBD-C18 column, 250 mm × 4.6 mm internal diameter, with 5 μm packing as the stationary phase at 25 °C. A mobile phase comprising methanol: 0.1% trifluoroacetic acid 80 : 20% v/v was used at a flow rate of 1.5 mL min^{-1} with the sample injection volume of 10 μL and run time of 7 min. The retention

time for diclofenac sodium was approximately 4.5 min with UV detection at a wavelength of 279 nm. Linearity was tested with a standard concentration range from 0.025 μg mL^{-1} to 500 μg mL^{-1} and evaluated using the coefficient of determination (R^2), with an R^2 value between 0.99 and 1 being acceptable.

Formulations

Compound **1** was suspended or dissolved in various solvent systems, including PBS (pH 7.4), dimethyl sulfoxide (DMSO) + PBS (pH 7.4), and DMSO + Transcutol, to evaluate the permeation of diclofenac sodium released from compound **1** through human cadaver skin. Pure diclofenac sodium dissolved in the same solvent systems was tested concurrently for comparative analysis.

Antimicrobial activity tests

Antimicrobial activities of the compound **1**, CSM, and **composite 1@CSM** were tested for the bacteria *Staphylococcus aureus*, *Escherichia coli*, and *Pseudomonas aeruginosa*, as well as for the yeast *Candida albicans.* The Minimum Inhibitory Concentration (MIC) of compound **1** was tested using the broth dilution method, following the procedures described by Grove and Randall.[24] For the assessment of contact activity of CSM and **composite 1@CSM**, suspensions (corresponding to 0.5 McFarland standard, diluted 1 : 10 with saline) prepared from the above-mentioned microorganisms cultured overnight on tripticasein soy agar (TSA) or sabouraud dextrose agar (SDA, both from BioMaxima, Lublin, Poland), were inoculated (28 μL each) on a set of discs made of the CSM as well as **composite 1@CSM**. The tests were carried out at T_0 (immediately after incubation and T_{24} (after a 24 h contact time of inoculum with the discs tested)). For the reading, the discs were flooded with 2.77 mL of D/E Neutralizing Broth (BioMaxima) and intensely vortexed for 2 minutes. To calculate the number of microorganisms, a series of ten-fold dilutions of the broth was inoculated onto TSA plates (for bacteria) or SDA (for *C. albicans*), and visible colonies were counted. Contact activity was estimated by comparison of colony numbers corresponding to T_0 and T_{24} for both supplemented and non-supplemented polymers.

Author contributions

Synthesis, S. W. J., J. M.; characterization, S. W. J., J. M.; conceptualization, S. W. J.; data analysis, J. M., S. W. J., S. R.; biological analysis, M. F., J. K.; skin studies, B. M.-K., S. R., S. R. T., N. A.; writing – original draft, S. W. J., J. M., B. M.-K., S. R., S. R. T, M. F., J. K.; writing – review and editing, S. W. J., B. M.-K., S. R.; project administration, S. W. J.; supervision, S. W. J. and B. M.-K.

Conflicts of interest

S. W. J. is listed as a co-inventor on patent application no. P.440906, which includes the synthesis of compound **1**.

Data availability

The supplementary information (SI) accompanying the submitted paper includes essential supporting data. Supplementary information: details on materials and methods, along with additional experimental results, such as IR, PXRD, ESI-MS, NMR and SEM data. See DOI: https://doi.org/10.1039/d5dt02494c.

Acknowledgements

S. W. J. acknowledges the financial support of the National Science Centre (Grant 2019/35/D/ST5/01155). Partial funding was provided by the Center for Dermal Research CDR at Rutgers, the State University of New Jersey, Piscataway, NJ, USA. We also thank MSc Marta Pawlicka for collecting the SEM data and Dr Miłosz Siczek for collecting PXRD data.

References

1 S. Kothawade and P. Shende, *Coord. Chem. Rev.*, 2024, **510**, 215851.
2 W. Chai, X. Chen, J. Liu, L. Zhang, C. Liu, L. Li, J. R. Honiball, H. Pan, X. Cui and D. Wang, *Regener. Biomater.*, 2024, **11**, rbad115.
3 E. Oheix, T. J. Daou and L. Pieuchot, *Mater. Horiz.*, 2024, **11**, 6222.
4 Y. Kong, Y. Sun, Z. Tian, S. Liu and N. Li, *Colloids Surf., B*, 2025, **252**, 114670.
5 K. Shang, C. Xu, Z. Cao, M. Cui, J. Sun, H. Xiao, L. Zhang, Y. Wang and H. Han, *Coord. Chem. Rev.*, 2024, **518**, 216071.
6 S. W. A. Shah, X. Li, H. Yuan, H. Shen, S. Quan, G. Pan, M. Ishfaq, A. U. Shah, H. Xie and J. Shao, *BMEMat*, 2025, e70001.
7 J. N. Murphy, J.-L. Kobti, M. Dao, D. Wear, M. Okoko, S. Pandey and V. N. Vukotic, *Chem. Sci.*, 2024, **15**, 7041.
8 X. Fu, T. Zhang, C. Xia, S. Du, B. Wang, Z. Pan, Y. Yu, P. Xue, B. Wang and Y. Kang, *Adv. Healthcare Mater.*, 2024, **13**, 2401788.
9 S. Mallakpour, E. Nikkhoo and C. M. Hussain, *Coord. Chem. Rev.*, 2022, **451**, 214262.
10 H. H. Balkhy, World Health Organization: Update on AMR —Developing a Fit for Purpose Response, 2021.
11 R. Gupta, V. Luxami and K. Poul, *ACS Appl. Mater. Interfaces*, 2025, **17**, 24830–24850.
12 A. Alshargabi, *J. Drug Delivery Sci. Technol.*, 2024, **95**, 105544.
13 C. Wang, J. Cheng, L. Song, Z. Zhou, Q. Zhao, Y. Zhao, H. Wang, Y. Tan, B. Zhao and M. Yang, *ACS Appl. Mater. Interfaces*, 2024, **16**, 29876–29890.

14 S. W. Jaros, U. K. Komarnicka, A. Kyzioł, B. Pucelik, D. S. Nesterov, A. M. Kirillov and P. Smoleński, *J. Med. Chem.*, 2022, **65**, 11100–11110.
15 S. Rashnoei, M. Shahamirian, S. Yazdanpanah and E. Ansarifar, *Sci. Rep.*, 2025, **15**, 11039.
16 A. Nadtochii and D. Baranenko, *Food Hydrocolloids*, 2024, **153**, 110051.
17 K. A. Weege, A. A. Ulson de Souza, A. C. Krause Bierhalz, P. Feuser and A. P. Serafini Immich, *ACS Omega*, 2024, **9**, 45591–45599.
18 V. Singh, K. Mahra, J. Klingate and J.-H. Shin, *Future Foods*, 2025, 100628.
19 T. Zare, A. Fournier-Level, B. Ebert and U. Roessne, *Ann. Bot.*, 2024, **134**, 725–746.
20 P. Mahajan, S. Nangare, A. Patil, P. Jain and L. Zawar, *Carbohydr. Polym. Technol. Appl.*, 2024, **7**, 100432.
21 S. Rashnoei, M. Shahamirian, S. Yazdanpanah and E. Ansarifar, *Sci. Rep.*, 2025, **15**, 11039.
22 M. Mujtaba, B. Koc, A. M. Salaberria, S. Ilk, D. Cansaran-Duman, L. Akyuz, Y. S. Cakmak, M. Kaya, K. M. Khawar, J. Labidi and S. Boufi, *Int. J. Biol. Macromol.*, 2019, **133**, 663–673.
23 J. Kong and S. Yu, *Acta Biochim. Biophys. Sin.*, 2007, **39**, 549–559.
24 D. C. Grove and W. A. Randall, Assay Methods of Antibiotic: A Laboratory Manual, in *Medical Encyclopedia*, New York, 1955.
25 S. W. Jaros, A. Krogul-Sobczak, B. Bażanów, M. Florek, D. Poradowski, D. S. Nesterov, A. M. Kirillov and P. Smoleński, *Inorg. Chem.*, 2021, **60**, 15435–15444.
26 S. W. Jaros, J. Król, B. Bażanów, D. Poradowski, A. Chrószcz, D. S. Nesterov, A. M. Kirillov and P. Smoleński, *Molecules*, 2020, **25**, 2119.
27 S. W. Jaros, F. M. C. Guedes da Silva, J. Król, M. C. Oliveira, P. Smoleński, A. J. L. Pombeiro and A. M. Kirillov, *Inorg. Chem.*, 2016, **55**, 1486–1496.
28 S. W. Jaros, M. Florek, B. Bażanów, J. Panek, A. Krogul-Sobczak, C. M. Oliveira, J. Król, U. Śliwińska-Hill, D. S. Nesterov, A. M. Kirillov and P. Smoleński, *ACS Appl. Mater. Interfaces*, 2024, **16**, 13411–13421.
29 A. C. Williams and B. W. Barry, *Adv. Drug Delivery Rev.*, 2012, **64**, 128–137.
30 B. C. Finnin and T. M. Morgan, *J. Pharm. Sci.*, 1999, **88**, 955–958.
31 J. Hadgraft and M. E. Lane, *Int. J. Pharm.*, 2005, **305**, 2–12.
32 M. E. Lane, *Int. J. Pharm.*, 2013, **447**, 12–21.
33 P. Karande and S. Mitragotri, *Biochim. Biophys. Acta, Biomembr.*, 2009, **1788**, 2362–2373.
34 K. Moser, K. Kriwet, A. Naik, Y. N. Kalia and R. H. Guy, *Eur. J. Pharm. Biopharm.*, 2001, **52**, 103–112.
35 N. Sathe, P. Beech, L. Croft, C. Suphioglu, A. Kapat and E. Athan, *Infect. Med.*, 2023, **2**, 178–194.
36 N. Gupta, K. Chauhan, G. Singh, S. Chaudhary and J. S. Rathore, *Microbe*, 2025, **6**, 100233.